# An automated method for identification and ranking of hyperspectral target detections

Bill Basener

Bill Basener, "An automated method for identification and ranking of hyperspectral target detections," Proc. SPIE 8048, Algorithms and Technologies for Multispectral, Hyperspectral, and Ultraspectral Imagery XVII, 80480D (20 May 2011); doi: 10.1117/12.885507

SPIE.

Event: SPIE Defense, Security, and Sensing, 2011, Orlando, Florida, United States

# An automated method for identification and ranking of hyperspectral target detections

Bill Basener

Rochester Institute of Technology
School of Mathematical Sciences
Rochester, NY, 14623, USA

## ABSTRACT

In this paper we present a new methodology for automated target detection and identification in hyperspectral imagery. The standard paradigm for target detection in hyperspectral imagery is to run a detection algorithm, typically statistical in nature, and visually inspect each high-scoring pixel to decide whether it is a true detection or a false alarm. Detection filters have constant false alarm rates (CFARs) approaching $10^{-5}$, but these can still result in a large number of false alarms given multiple images and a large number of target materials. Here we introduce a new methodology for target detection and identification in hyperspectral imagery that shows promise for hard targets. The result is a greatly reduced false alarm rate and a practical methodology for aiding an analyst in quantitatively evaluating detected pixels. We demonstrate the utility of the method with results on data from the HyMap sensor over the Cooke City, MT.

**Keywords:** hyperspectral, remote sensing, target detection, ATR, unmixing, on board processing, automated processing

## 1. INTRODUCTION

The goal of target detection is to determine which, if any, pixels in a hyperspectral image contain known spectra from a target or set of targets. The most common context, particularly for defense and security applications, is where the target is rare in the image and possibly subpixel. The standard process is to apply a detection algorithm to each pixel and use the output to decide if the target is present.[1] This decision is made, in theory, by setting a threshold on the output of the detector and declaring that every pixel scoring above the threshold contains target. Each declared pixel would be manually inspected to determine if the detection is real. We will refer to this process as the standard paradigm. The focus in recent years has been on improving detection algorithms[1–7] and methods for choosing the threshold value to obtain a given constant false alarm rate (CFAR)[4,8,9] which is the number of false alarms per image pixel. A CFAR of $10^{-5}$ is considered a suitable goal.

One of the interesting results from experiments has been that detector performance varies greatly with choice of preprocessing and detector algorithm choices as well as target material,[7,10–12] and that a theoretical CFAR on the order of $10^{-5}$ is not robustly achievable without greatly sacrificing detection rates. While the search for a better detector has resulted in algorithms that sometimes outperform the standard ACE and matched filter, the search for a single detection algorithm that can create detection planes with sufficient accuracy for real-time target detection and analysis has not been successful. Some evaluation of new detection algorithms suggests that the apparent improvement in test situations does not translate into robust improvement in realistic applications.[6] A best robust performer may be an ACE algorithms with a properly computed covariance matrix, which has been shown to have good performance over multiple targets in full images.[7,11] Moreover, even if it were robustly achievable, a CFAR threshold of $10^{-5}$ is not truly practical, demonstrated in the example below.

To understand the practical deficiencies of the standard paradigm, consider the following example. Five target materials, let's call them T1, T2, T3, T4 and T5 for now, were used as targets in the matched filter detection algorithm applied to run 05m51 from the Forest Radiance data set[13] and the resulting detection planes are shown in Figure 1. This image was acquired with the HYDICE sensor with a ground sample distance of about 0.9m. It was atmospherically corrected with the empirical line method and after removing noisy/water bands 145 bands remained. The wavelengths range approximately from 400nm to 2500nm. The portion of the full image has 800 lines (rows) and 320 samples (columns).

Algorithms and Technologies for Multispectral, Hyperspectral, and Ultraspectral Imagery XVII,
edited by Sylvia S. Shen, Paul E. Lewis, Proc. of SPIE Vol. 8048, 80480D · © 2011 SPIE
CCC code: 0277-786X/11/$18 · doi: 10.1117/12.885507

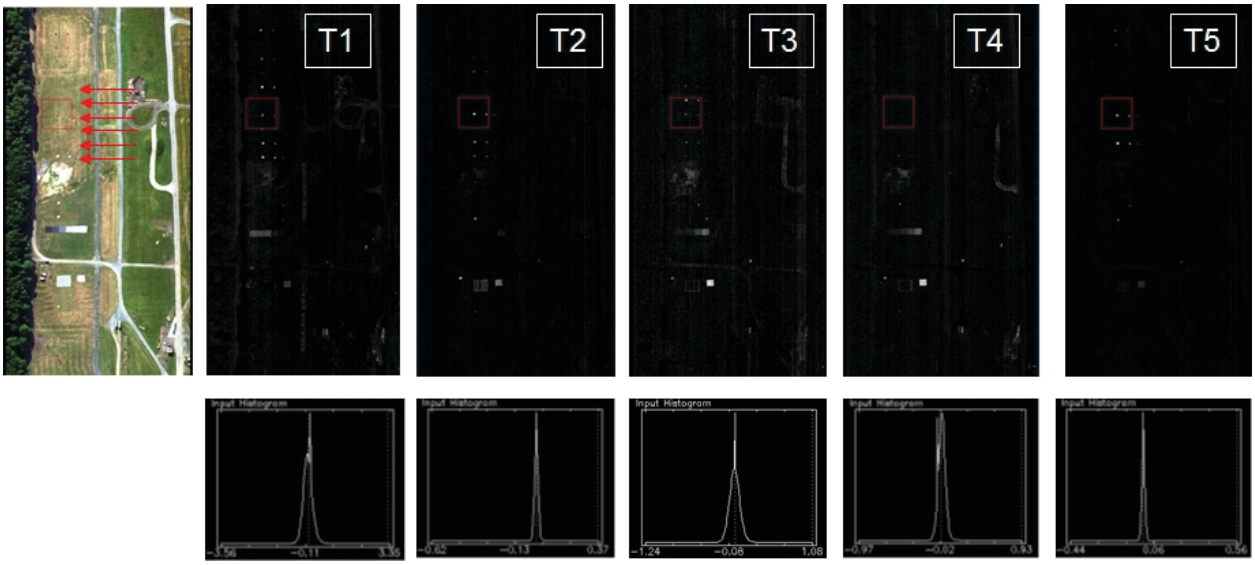


Figure 1. Detection planes with histograms for five materials using imagery from the Forest Radiance data set. The arrows in the RGB image indicate the locations of fabric targets F2, F3, F4, F5, F11 and F12, from bottom to top. For each fabric type, there are 3 panels arranged in a horizontal row from largest (left) to smallest (right).

Various bright objects in the detection planes are potential real detections. From the histograms, we see that T1 has a maximum matched filter score of 3.35. This is extremely high, as the MF is supposed to correspond to abundance with a theoretical maximum of 1. While factors such as variation in illumination may legitimately result in scores a little above 1, a score is 3.35 indicates that something is not appropriate for a real detection. Target T2 has a maximum detection score of 0.37, which would be likely to be below a CFAR threshold, T3 and T4 have top scores close to 1, which suggest real detections, and T5 has a top score of 0.54 which is reasonable for a borderline detection on an object with a 50% pixel abundance. Given this information alone, it is difficult, perhaps impossible, to determine with accuracy which pixels in these images correspond to actual detections of the target. At best, one could proceed with the time-consuming task of inspecting all spectra for high-scoring pixels to make decisions.

The materials used are cinders (T1), the Forest Radiance F2 target (T2), Terra Cotta Tile (T3), Concrete (T4) and the Forest Radiance F3 target (T5). All of the bright pixels in the T1 plane are false alarms. For T2, only the row of panels indicated as F3 on the RGB image are real detections - all other bright objects are false alarms. All bright pixels in the T3 detection plane are false alarms. In the T4 detection plane, the road pixels might be considered legitimate detections since the material is concrete, while the other bright pixels are false alarms. For the T5 detection plane, the real targets are the row of panels indicated as F3 on the RGB image. The ability to make these determinations is not present in the matched filter detection planes by themselves.

The purpose of the above demonstration is to identify the practical deficiencies of the standard method. The targets above were chosen to illustrate the deficiencies, as only two of the target materials were actually targets in the image. Also, the matched filter detection algorithm is known the be false alarm prone. The results would not have looked so bad using the detection planes from ACE. However, this demonstration actually underestimates the problem, rather than overstating it.

Consider a more practical situation, where one is looking for ten target materials. For each material, multiple target spectra should be included in the library to allow for variation such as weathering, contaminants and other factors. (If one is looking for a given plant species it is useful to take measurements of the plant in different stages of development and health. For vehicles, it can be useful to have spectra off different parts of the vehicle in different variations that one would expect to encounter. In searching for lost campers, as another example, one might use spectra for each of the plastic or nylon objects such as coolers and tents and that the campers would be likely to have.) Thus one could easily have 100 or more spectra. For a search situation, the sensor should be collecting data wherever the target(s) could possibly be found. Thus, it is easy to have situations

where 100 or more images would be collected per day. (An image of the size shown in Figure 1 can take less than one minute to collect, and 100 images of this size would cover approximately 25 square kilometers.) Thus, we could easily have 10,000 detection planes to examine per day, instead of the 5 used in the demonstration. A CFAR threshold of $10^{-5}$ would result in roughly 5 false alarms per image, resulting in 50,000 false alarms per day (or 2,000 per square kilometer.)

In this paper we avoid the need for a detection algorithm that creates sufficiently accurate detection planes and suggest a paradigm shift to a more thorough process involving a detection step and an identification step. The main idea of our methodology is simple: we run a standard target detection to obtain detections planes, choose high-scoring pixels from the planes, apply further "identification algorithms" to the high scoring pixel and local region, and then output a list of results that can be sorted by the scores from the identification process. This is a paradigm shift from the standard processing methodology, being object-based in the sense that the user examines a list of regions in the image with information about the object in each region, instead of pixel-based, with the user visually examining the scores in detection planes for each pixel. Because the identification step is only applied to a small fraction of pixels from the image, it can include powerful but time consuming algorithms and large libraries that would be impractical or impossible to apply to every pixel in an image. The result is much higher confidence results with much less human interaction time in comparison to that of standard methods.

### 1.1 Data

The data used in this analysis was collected by the HyMap sensor over the Cooke City, MT area on July 4, 2006.[14] These data have 126 usable bands (after the atmospheric absorption bands are removed) between 450nm and 2500nm with 2.5m ground sample distances (GSD) (Figure 2.) We removed 4 additional bands for a total of 122 bands. Ground truth, including the location and spectra for the cloth and vehicle targets, is freely available at.[15]

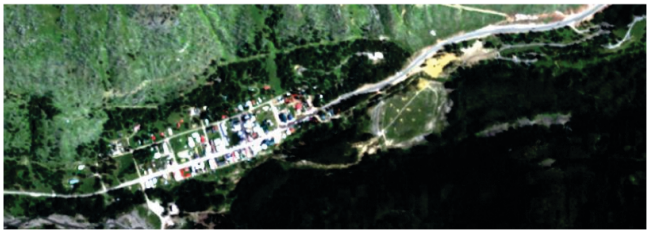

Figure 2. True color image of Cooke City, MT.

## 2. DETECTION, IDENTIFICATION AND PRESENTATION

Our proposed methodology has three separate stages. First, a target detection algorithm is applied to the image using the known target(s) in the usual sense. Second, each high-scoring pixel (one could use a spatial group of pixels, but we just use the highest scoring pixel) is run through an identification (ID) algorithm. The goal of the ID algorithm is to reduce false alarms and enable confident determination as to the validity of the detected pixel. Third, the results are sorted in such a way as to make the results useful in practical search applications. We do not contend that any of our implementation of the steps individually is optimal, but that it is the process as a whole that can enable practical exploitation of hyperspectral imagery for search.

### 2.1 Detection

For the detection process, we use a slight modification of the standard ACE (adaptive coherence/cosine estimator) detection algorithm,

$$ACE(x) = \frac{x\Sigma^{-1}t}{\sqrt{x\Sigma^{-1}x}\sqrt{t\Sigma^{-1}t}},$$

where $\Sigma$ is the covariance matrix, $t$ is the target of interest, and $x$ is the test pixel. We compute the covariance matrix by first running an anomaly detection algorithm and using the 90% of pixels with the lowest RX score

(least anomalous) for the computation of the covariance. The threshold of 90% is somewhat arbitrary and we use RX so others can reproduce our results. The Topological Anomaly Detector (TAD) provides a percentage of the image that corresponds to background and performed better than RX for computing statistics in some previous tests.[7] Computing ACE with the anomaly removed covariance, or with otherwise modified statistics, has proven to be a relatively solid performing algorithm.[7,11] We call this algorithm RX-ACE.

### 2.2 Identification

Suppose that for each target in our library, a detection plane has been creating using the RX-ACE algorithm. We convert each detection plane to units of standard deviation ($\sigma$) from the mean. Only pixels that have a sufficiently high detection score proceed to the identification step. (We used a threshold of $3\sigma$.) Even if a pixel scores above the threshold for multiple detection targets, it will be passed only once to the identification step. This is one of the advantages of performing an automated detection-identification process; the detection planes for the multiple spectra do not need to be individually inspected.

One a high-scoring detected image pixel is selected, it passes to the identification (ID) step. The goal of the ID step is to determine which spectrum (or spectra) in an identification library is (are) most likely to be in the pixel. The identification step uses an identification library, which is typically much larger than the target library, possibly including multiple variations of target such as field measurements, lab measurements and in-scene spectra from previous images. Our ID step has two parts. First we compute the ACE score using the spectrum from the selected high-scoring image pixel and all spectra in the identification library. The spectrum from this library with the highest detection score is called the identification spectrum for that pixel. Then we perform an unmixing process (described in detail below) to compute an error metric and subpixel spectral plots that can be use to filter false alarms. Because this identification step is performed on only a relatively few number of pixels (say, up to 100 pixels per image), the identification library could contain a thousand or more spectra and could include modified spectra from MODTRAN computations with varying parameters to account for targets in shadow or imperfect atmospheric compensation. (We used the same library for detection and identification, which included just the spectra from the self test portion of the provided data.)

Using an identification process is not new; in longwave hyperspectral imagery, identification is a standard process but is performed manually only when a potential target is identified by a user. The goal in that case is to determine the correct combination of gasses that are present in a plume, not detect a single material. Our contribution is that automating this process and using the output to sort and prioritize detections provides enormous benefits in both processing time and accuracy. Our identification algorithm, the algorithm that we use to match the pixel to spectra in the identification library, is just the standard ACE detector followed by a local unmixing to estimate error. This leaves the option open for future work on improved identification algorithms, (e.g., linear regression methods), that provide more accuracy with a runtime of seconds per pixel. Similarly, one could use the location of the flagged pixel from the hyperspectral image to initiate processing in co-registered data from other modalities such as LIDAR or high resolution imagery.

The linear unmixing with endmembers process that we used is as follows:

1. A spatial tile (we used a square with radius equal 15 pixels) centered around the detected pixel is selected.
2. All pixels scoring above some threshold (in this case, $1\sigma$) are masked out.
3. Endmembers $\mathbf{e_1}, \mathbf{e_2}, ..., \mathbf{e_K}$ are computed from the non-masked pixels, where $K$ is initially 10.
4. Linear unmixing is performed using the $K$ endmembers and target spectrum to create a model

$$\mathbf{M_K} = c_t\mathbf{t} + \sum_{k=1}^{K} c_k\mathbf{e_k}.$$

5. The background of the model is $\mathbf{b} = \sum_{k=1}^{K} c_k\mathbf{e_k}$ and the background-removed pixel is $\mathbf{x} - \mathbf{b}$

6. The unmixing error $error_K = \left|\left| \frac{(\mathbf{x}-\mathbf{b})}{|\mathbf{x}-\mathbf{b}|} - \frac{\mathbf{t}}{|\mathbf{t}|} \right|\right|$ is computed. This error is the area between the background-removed pixel and target spectra once both are normalized.

7. The endmember with the lowest abundance is removed. Steps 4 and 5 are repeated iteratively to find models $M_{10}, ..., M_0$ with error $error_{10}, ..., error_0$.

8. The model with the least error is chosen as the "best model" for this pixel as a mixture between the target spectra and local background. (The method for reducing endmembers used here is similar to that used in.[16])

From this process we obtain the error for the best model which can aid in determining a confidence level for the detection. Also, for the model with lowest error, we can have computed the background-subtracted spectrum, $\mathbf{x} - \mathbf{b}$, which can be plotted along with the identification spectrum as a way to perform visual spectroscopy on a subpixel detection.

The identification step, including computing the best match between the pixel spectrum and the identification library and the unmixing with local endmembers, is run iteratively on high-scoring pixels in the image beginning with the highest-scoring pixel. To avoid running identification on multiple pixels on the same object, some spatial processing is used. A small local window of pixels (we used a square of radius 3) centered on the target pixel is masked out of the detection planes for all pixels and a larger window (we used a square of radius 6) is masked out of the detection plane for the material in which the pixel had its highest-scoring detection. After masking out these pixels, the next highest scoring pixel in the detection planes is put though the identification process, and we repeat until all pixels scoring above a fixed threshold (we used $3\sigma$) are identified.

The identification process results in the following information for the pixel: ACE scores with spectra from the identification library, unmixing percentage in the best model and error from the best model. In addition, we compute the background-removed spectrum $\mathbf{x} - \mathbf{b}$. To aid in spectroscopic evaluation of the pixel, we plot the pixel spectra $\mathbf{x}$, the identification spectra, and the scaled background-removed spectrum $(\mathbf{x} - \mathbf{b})\frac{|\mathbf{t}|}{|\mathbf{x}-\mathbf{b}|}$, as shown in Figure 3.

## 3. RESULTS

The target detection-identification methodology was applied to the Cooke City dataset described in Section 1.1. The number of false alarms for each target are provided in Table 1. For the detection algorithm RX-ACE, the number provided is the number of pixels scoring higher than the pixel provided in the ground truth for that target. The number provided in the table for the detection-identification process is the number of identified pixels for which the identification score is higher than that for the ground truth pixel. (The identified pixels are ranked according to RX-ACE score, as RX-ACE was used as the identification algorithm.)

Table 1. Number of false alarms for various detectors. (Not available (NA) indicates that the detection was below the $3\sigma$ threshold.)

| Target | RX-ACE | Detect-Id |
|---|---|---|
| Red Cotton 2m | 0 | 0 |
| Yellow Nylon 2m | 0 | 0 |
| Blue Cotton 2m | 0 | 0 |
| Red Nylon 2m | 0 | 0 |
| Green Vehicle | 336 | 1 |
| White Vehicle | 7270 | NA |
| Red Vehicle | 1091 | NA |

The reduction on false alarms evident in Table 1 is the result of spatial processing - that we masked all high scoring pixels around the highest scoring pixel for the green SUV. All of the false alarms for the RX-ACE algorithm are pixels on a green steel roof, which only count as one object in the detection-identification process.

In addition to this reduction in false alarms, the unmixing from the identification process enables some distinction between identifications of real targets and false alarms that scored roughly as high as the real pixels.

In addition to sorting the results for easy viewing, the identification process provides the subpixel spectrum; that is, the spectrum obtained by subtracting off the background from the unmixing model as described in Section 2.2. This spectrum aides in human verification of a detection. Figure 3 shows the pixel spectrum (red), the red cotton target spectrum (black) and the background-subtracted pixel (blue) for the detection on the red cotton target. Observe that comparison of the target spectrum to the pixel spectrum (red to black) does not provide evidence for a real detection, but the background-removed spectrum is a good match to the target (blue to black), providing supporting evidence for this detection. For comparison, the corresponding spectra for a 'false alarm' on a the same target is shown in Figure 4; notice that the background-removed pixel to target (blue to black) is not as good of a match as in the real detection in Figure 3. For applications in which visual confirmation of spectra is required, the standard methodology is of no use for subpixel detection but the background-removed spectra in this paper enable such confirmation.

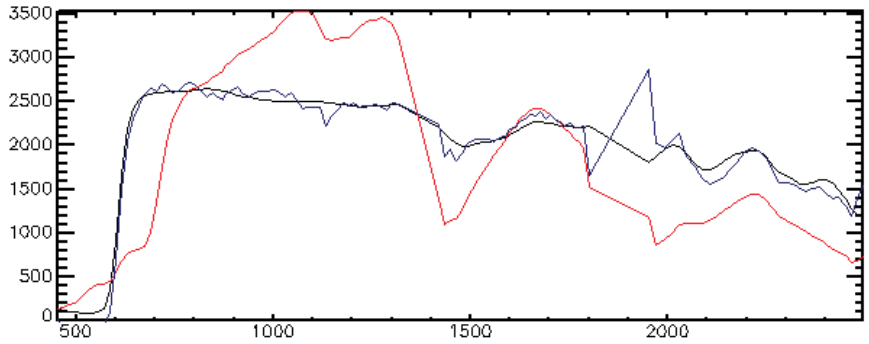


Figure 3. The pixel spectrum (red), target spectrum (black) and background-removed pixel spectrum (blue) for the detection on the red cloth target. The ACE score for this pixel is 0.94 and the error is 7%. Note the good blue-to-black (subpixel) spectral match indicating a true detection.

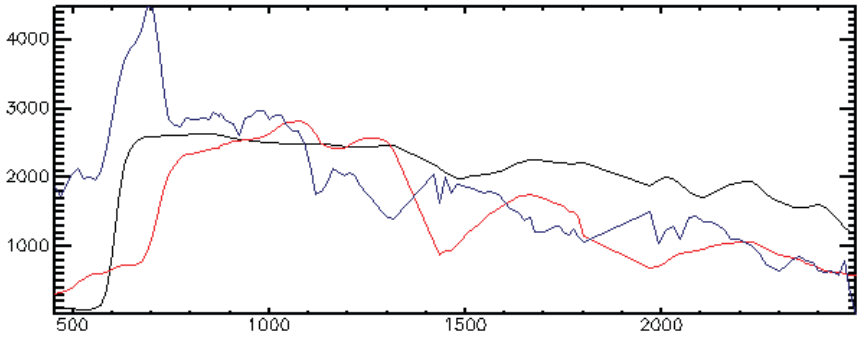


Figure 4. The pixel spectrum (red), target spectrum (black) and background-removed pixel spectrum (blue) for a pixel scoring nearly as high as the real target for the red cotton. The ACE score for this pixel is 0.79 and the error is %44. Note the poor blue-to-black (subpixel) spectral match indicating a false alarm.

The associated spectra for the pixel on a harder target, the green SUV, is shown in Figure 5. (This is the pixel on the ROI for this target from the ground truth and it is the second highest scoring identified location in our algorithm.) Note that the ACE score for the real green SUV and the false alarm in Figure 4 are both 0.79. In units of standard deviations, the identification of the green SUV is lower (at $7.2\sigma$) in comparison to that of the false alarm ($8.1\sigma$). In this case, the lower error from the ID step on the green SUV and better subpixel spectral match indicates that Figure 5 is on the real target while Figure 4 is a false alarm.

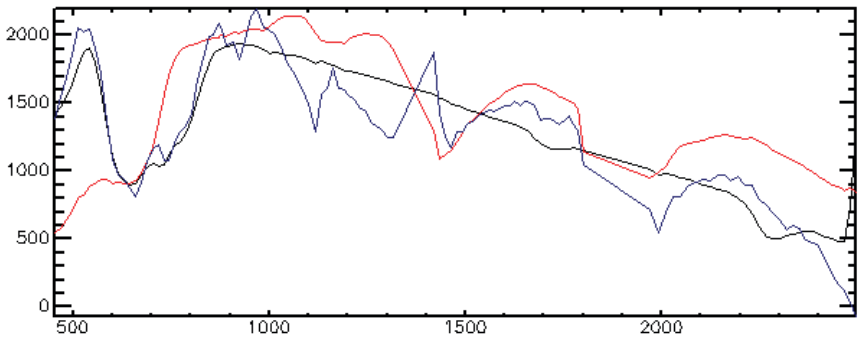


Figure 5. The pixel spectrum (red), target spectrum (black) and background-removed pixel spectrum (blue) for the pixel on the green SUV. The ACE score for this pixel is 0.79 and the error is %17. Note the good blue-to-black (subpixel) spectral match indicating that this is a good identification.

## 4. CONCLUSION

We demonstrated that the detection-identification process provides potential for reduced human interaction time for target detection in hyperspectral imagery. In the Cooke City dataset, we demonstrated a reduced false alarm rate using this methodology, particularly in applications which require visual confirmation of spectra. Our test was limited in scope; we did not rigorously evaluate the utility of the error metric as a tool for false alarm reduction over a large number of targets and we did not employ a large library with background spectra. Our identification algorithm is just applying the ACE algorithm to the pixel with a potentially larger identification library. This suggests several options for future work: development and implementation of better identification algorithms, use of larger libraries including more variations of the target spectra and more substantial testing of the methodology. The most important of these is probably to develop a better identification process, perhaps one that can incorporate the local unmixing methods as together with statistical scores.

## REFERENCES

1. D. Marden D. Manolakis and G. Shaw, "Target detection algorithms for hyperspectral imaging application," 2003, vol. 14(1) of *Lincoln Laboratory Journal*, p. 79116.
2. A. Schaum, "Spectral subspace matched filtering," 2001, vol. 4381 of *Proc. SPIE*.
3. A. Schaum, "Hyperspectral detection algorithms: Operational, next generation, on the horizon," 2005, IEEE Computer Society, 34th Applied Imagery Pattern Recognition Workshop.
4. M. Rossacci R. Lockwood T. Cooley D. Manolakis, D. Zhang and J. Jacobson, "Maintaining cfar operation in hyperspectral target detection using extreme value distributions," 2007, vol. 6565 of *Proc. SPIE*.
5. T. Cooley D. Manolakis, R. Lockwood and J. Jacobson, "Target detection algorithms for hyperspectral imaging application," 2009, vol. 733402 of *Proc. SPIE*.
6. T. Cooley D. Manolakis, R. Lockwood and J. Jacobson, "Is there a best hyperspectral detection algorithm?," 2009, vol. 7334, 733402 of *Proc. SPIE*.
7. W. Basener, "Clutter and anomaly removal for enhanced target detection," 2010, vol. 7695, 769525 of *Proc. SPIE*.
8. D. Marden and D. Manolakis, "Modeling hyperspectral imaging data using elliptical contoured distributions," 2003, vol. 5093 of *Proc. SPIE*.
9. A. Schaum, "Adapting to change: The cfar problem in advanced hyperspectral detection," 2007, IEEE Computer Society, 36th Applied Imagery Pattern Recognition Workshop.
10. J. Kerekes D. Grimm, D. Messinger and J. Schott, "Hybridization of hyperspectral imaging target detection algorithm chains," 2005, vol. 5806, 753 of *Proc. SPIE*.
11. M. Halper, "Global, local, and stochastic background modeling for target detection in mixed pixels," 2010, vol. 7695, 769527 of *Proc. SPIE*.
12. R. Resmini and M. Salvador, "Comparison of spectral matching techniques for vegetation species delineation of the national arboretum," 2009, vol. 7334 of *Proc. SPIE*.

13. S. Bergman R. Olsen and R. Resmini, "Target detection in a forest environment using spectral imagery," 1997, vol. 3118, 46 of *Proc. SPIE*.
14. I. Fairweather R. Crabtree J. Shive D. Snyder, J. Kerekes and S. Hager, "Development of a web-based application to evaluate target finding algorithms," in *IEEE Trans. Geosci. Rem. Sens.*, 2008, [DOI: 10.1109/IGARSS.2008.4779144].
15. "Target detection blind test," http://dirsapps.cis.rit.edu/blindtest/.
16. J. Greer, "Sparse demixing," 2010, vol. 7695 of *Proc. SPIE*.